RAC1B function is essential for breast cancer stem cell maintenance and chemoresistance of breast tumor cells

Ahmet Ucar (ahmet.ucar@manchester.ac.uk)
University of Manchester https://orcid.org/0000-0002-6551-3486
Fuhui Chen
David Novo
Denis Alferez
Kyriaki Pavlou
Jingwei Zhang
University of Manchester
Secil Eroglu
Neil Humphreys
Antony Adamson
Andrew Campbell
CRUK Beatson Institute https://orcid.org/0000-0003-3930-1276
Cathy Tournier
University of Manchester https://orcid.org/0000-0002-4618-2570
Robert (B.) Clarke
University of Manchester https://orcid.org/0000-0001-5407-3123
Keith Brennan
University of Manchester https://orcid.org/0000-0002-9384-125X
Charles Streuli

Article

Keywords:

Posted Date: April 15th, 2022

DOI: https://doi.org/10.21203/rs.3.rs-1343371/v1

Version of Record: A version of this preprint was published at Oncogene on January 5th, 2023. See the published version at https://doi.org/10.1038/s41388-022-02574-6.

Abstract

Breast cancer stem cells (BCSC) are presumed to be responsible for treatment resistance, tumor recurrence and metastasis of breast tumors. However, development of BCSC-targeting therapies has been held back by their heterogeneity and the lack of BCSC-selective molecular targets. Here, we demonstrate that Rac1b, the only known alternatively spliced variant of the small GTPase Rac1, is expressed in a subset of BCSCs in vivo and its function is required for the BCSC maintenance and the chemoresistance of breast tumor cells. In human breast cancer cell line MCF7, RAC1B is required for BCSC plasticity and chemoresistance in vitro and for tumor-initiating abilities in vivo. Unlike Rac1, Rac1b function is dispensable for normal mammary gland development and mammary epithelial stem cell (MaSC) activity. In contrast, loss of Rac1b function in a mouse model of breast cancer hampers BCSC activity in vivo and increases the chemosensitivity of primary tumor cells to doxorubicin. Collectively, our data suggest that RAC1B is a clinically relevant molecular target for the development of BCSC-targeting therapies that will improve the effectiveness of currently available chemotherapy modalities.

Introduction

Breast cancer is the most common cancer in women and the fourth leading cause of cancer-related deaths in the world [1]. Despite the advances in clinical treatment options for patients with breast cancer, tumor recurrence and therapy resistance are still significant and contribute to high mortality rates. Breast cancer stem cells (BCSC), also known as tumor-initiating cells, are presumed to be responsible for therapy resistance, tumor recurrence and metastasis. Therefore, BCSC-targeted therapies could have a potential to improve clinical outcomes. However, the development of such therapies is complicated by the BCSC heterogeneity, which is driven by the intrinsic stem cell plasticity, and the lack of knowledge on BCSC-specific molecular targets that are dispensable for normal adult stem cells [2].

RAC1 is a small GTPase that functions as a key signalling node downstream of various microenvironmental signalling pathways, including those triggered by cell adhesion and growth factors. RAC1 signalling is upregulated in various cancers, including breast cancer[3-7], and regulates cellular processes such as tumor cell survival, proliferation and invasion [8]. Importantly, RAC1 is implicated in therapy resistance of tumor cells against both cytoablative [9-11] and targeted treatments [9, 12-16]. However, due to its almost ubiquitous expression and critical functions in the development and homeostasis of various organ systems [17-20], there is little clinical relevance of potential RAC1-targeted treatments. Hyperactivation of RAC1 signalling in tumors is associated with rare mutations, upregulated expression or misregulation by RAC1-regulatory proteins including Guanine-nucleotide exchange factors (GEFs), GTPase-activating proteins (GAPs) and Guanine-nucleotide dissociation inhibitors (GDIs) [7, 8, 21-23].

Hyperactivation of RAC1 signalling in some solid tumors is in part due to the alternative splicing of *RAC1* to generate the RAC1B variant, a constitutively active form of the small GTPase [24-26]. RAC1B has an additional exon (i.e. exon3b) encoding 19 amino acids with an in-frame insertion just after its Switch-II

domain. This leads to a structural change favouring the active GTP-bound state independent of GEF-mediated activation [27]. Previous studies have suggested that RAC1B is a tumor-specific splice variant of RAC1, as its expression during organogenesis ceases in adulthood and only gets upregulated in some solid tumors [24].

In this study, we have used human breast cancer cell line MCF7 and genetically engineered mouse models to demonstrate that, unlike Rac1, Rac1b function is dispensable for normal mammary gland development and mammary epithelial stem cells (MaSCs). In contrast, Rac1b is required for BCSC plasticity and maintenance as well as chemosensitivity of breast tumor cells. Furthermore, by generating a new knock-in mouse line serving as a surrogate reporter for Rac1b splicing, we have identified Rac1b as a marker of a substantial subset of BCSCs, indicating a potential stem cell heterogeneity in mammary tumors. Our results propose RAC1B as a promising molecular target in sensitising breast tumors to chemotherapy, potentially due to its function in regulating BCSC plasticity and self-renewal, and thus provides a clinically relevant molecular target for developing BCSC-targeting therapies.

Results

BCSCs require RAC signaling for their self-renewal maintenance

We have previously shown that Rac1 is required for MaSC self-renewal [18]. In order to elucidate whether RAC signaling is also required for BCSC activity, we used two specific RAC-inhibitors with different modes of action in the mammosphere culture of human breast cancer cell lines that are known to generate proliferation-driven mammospheres [28]. These lines represent different breast cancer subtypes: Luminal-A (MCF7 and T47D), Luminal-B (BT474), and HER2+ (JIMT-1). The inhibitors render RAC proteins in a nucleotide-free inactive state (EHT-1864) or prevent the RAC activation by GEFs (EHop-016) [29, 30]. Interestingly, the mammosphere-forming ability of these cell lines was completely abrogated in the presence of either EHT-1864 or EHop-016 (Figure 1A,B).

Mammosphere formation requires an initial self-renewing division of the stem cell, followed by consecutive rounds of proliferation of their non-stem cell progeny generating all other cells within the mammosphere [31]. Therefore, we asked whether RAC inhibition results in depletion of BCSCs or inhibition of cell proliferation, both of which could prevent mammosphere formation. To address this question, we treated MCF7 cells with RAC inhibitors in the primary mammosphere culture for 5 days and then performed a secondary mammosphere formation assay in the absence of inhibitors. If the effect of RAC inhibition on primary mammosphere formation is due to inhibition of cell proliferation, BCSCs would be able to initiate the secondary mammosphere formation when RAC inhibitors are removed. Our results demonstrated that RAC-inhibited MCF7 cells did not form any secondary mammospheres despite the absence of RAC inhibitors (Figure 1C). This suggests that RAC inhibition results in BCSC depletion.

We also tested whether RAC inhibition affects the proliferation of the non-stem cell progeny of BCSCs. To this end, we added RAC inhibitors to the mammosphere culture of MCF7 cells at the time of plating (0 hours) or 24 hours after plating. Our results showed that the effect of RAC inhibition is restricted to the

initial cell divisions of BCSCs that take place within the first 24 hours of culture, whereas the proliferation of non-stem cell progeny of BCSCs does not rely on RAC signalling (Figure 1D). At higher concentrations of RAC inhibitors, there was a cell-shedding phenotype rather than a slow growth of mammospheres. A similar cell-shedding phenotype also occurs when fully formed mammospheres at Day 5 of culture are treated with high concentrations of these inhibitors (data not shown), suggesting a potential inhibition of cell-cell adhesion in the presence of higher concentrations of inhibitors.

Since BCSCs play essential roles in breast tumorigenesis, we examined whether Rac1 is required for breast tumorigenesis *in vivo*. We generated a double transgenic mouse line bearing floxed-*Rac1* allele [32] and MMTV-Neu-IRES-Cre (NIC) transgene [33], which allows genetic deletion of *Rac1* in the same cells that overexpress Neu oncogene. Tumor latency analysis reveals that heterozygous deletion of *Rac1* in $Rac1^{flox/+}$;MMTV-NIC mice significantly delays the palpable tumor formation compared with $Rac1^{+/+}$;MMTV-NIC mice (Figure 1E). Although we were able to obtain only two female $Rac1^{flox/flox}$;MMTV-NIC mice, only one of them has developed palpable tumors during its first year of age (Figure 1E). Since Rac1 is indispensable for early-stage embryogenesis [34], it is likely that leaky expression from the MMTV promoter during early embryogenesis led to *Rac1* deletion and thus embryonic lethality in most of the $Rac1^{flox/flox}$;MMTV-NIC embryos.

These results reveal that RAC signalling is required for the self-renewal maintenance of BCSCs *in vitro*, and that loss-of Rac1 function delays or supresses breast tumorigenesis in a dose-dependent manner *in vivo*.

RAC1B influences BCSC plasticity

Since RAC inhibitors and Cre-mediated genomic deletion of *Rac1* result in the loss of both RAC1 and RAC1B functions [35, 36], we decided to investigate to which extent the observed phenotypes would be recapitulated by targeting only RAC1B. Initially, we analysed whether RAC1B is expressed in human breast cancer cell lines, murine mammary gland, and breast tumors of MMTV-NIC mice (Supplementary Figure 1). RAC1B mRNA and protein are present in ER+ cell lines, and low levels of RAC1B protein was also observed in the HER2+ cell line JIMT1. In contrast, RAC1 mRNA and protein are present in all 5 cell lines tested, though RAC1 protein levels are higher in HER2-overexpressing cell lines BT474 and JIMT1. In mice, Rac1b mRNA was detected predominantly in the basal mammary epithelial cells at adult nulliparous and early-pregnancy stages, and in the MMTV-NIC tumor cells (Supplementary Figure 1).

To determine whether variant-specific loss of RAC1b affects BCSCs, we employed CRISPR/Double-nickase method to target the exon3b-encoding genomic sequence in MCF7 cells (Figure 2A). This was followed by single-cell cloning to ensure the genomic homogeneity of clones for further phenotypic analyses. We obtained several single-cell clones that specifically lacked RAC1b mRNA (Figure 2B) and protein (Figure 2C). Sequencing of the targetedgenomic locus in these clones revealed distinct insertion/deletion (indel) mutations in each allele of each clone (Figure 2A). Interestingly, even small

deletions within the exon3b-coding sequence resulted in the loss of RAC1B mRNA, suggesting that those deletions may have disrupted the splicing-regulatory sequences required for *RAC1B* splicing.

We found that the loss of RAC1B function in these MCF7 clones did not alter their mammosphere-forming capacity (Figure 2D), although it caused a significant increase in the frequency of their Aldefluor^{bright} BCSC population as determined by flow cytometry (Figure 2E). To address whether gain of RAC1B function leads to an inverse phenotype, we generated stable transgenic MCF7 clones with doxycycline-inducible expression of RFP-RAC1B fusion protein (Figure 2F). Similar to the RAC1B-null MCF7 clones, the RAC1B overexpression did not alter MCF7 mammosphere-forming capacity (Figure 2G). However, it resulted in a significant increase in the CD44^{+};CD24^{-} BCSC population (Figure 2H).

Earlier studies have described Aldefluor^{bright} and CD44^{+};CD24^{-} populations in MCF7 cells as the proliferative epithelial-like and quiescent mesenchymal-like states of BCSCs, respectively, and suggested that the ability to reversibly transit between these states underlies the plasticity within the BCSC pool [37, 38]. Our results therefore suggest that RAC1B regulates the reversible switching between the proliferative versus quiescent states of BCSCs without altering the total BCSC numbers and it is likely to be required for the quiescent BCSC state.

RAC1B function is essential for chemoresistance and *in vivo* tumor initiating ability of MCF7 cells

Resistance to chemotherapy is a feature often attributed to CSCs. As cytoablative treatments specifically target proliferating cells, quiescent CD44^{+};CD24^{-} BCSCs are likely to constitute the chemoresistant population of tumor cells. Given that RAC1B function might be required for this particular BCSC subpopulation, we hypothesised that RAC1B may have a crucial role in chemoresistance. We therefore determined the effect of doxorubicin on RAC1B-null and RAC1B-overexpressing MCF7 cells. We treated these cells with 2.5 uM doxorubicin for 24 hours, which led to more than 90% of cell loss, and then measured the recovery as cell growth in the absence of doxorubicin. Parental MCF7 and RAC1B-proficient MCF7 clone (Clone-22) showed a slow but steady recovery during the five-day period after doxorubicin removal (Figure 3A). In contrast, RAC1B-null MCF7 clones did not recover during the same period (Figure 3A) nor up to 3 weeks post-treatment (data not shown). Conversely, the RAC1B-overexpressing cells showed a robust recovery upon doxorubicin withdrawal (Figure 3B) compared with the same cells not treated with doxycycline to induce RAC1B overexpression. These results indicate that RAC1B function plays a crucial role in the chemoresistance of MCF7 cells *in vitro*, possibly through its effect on BCSC plasticity.

Since impaired BCSC plasticity may alter tumorigenesis, we investigated whether RAC1B is required for tumor-initiating ability of BCSCs *in vivo*. Xenograft transplantation of parental MCF7 cells resulted in visible tumor formation within 6–7 weeks (Figure 3C). In contrast, RAC1B-null MCF7 clones formed no visible tumors, even up to 100 days post-transplantation. At the experimental endpoint (either maximum tumor burden of 1.25 cm^3 or 100 days post-transplantation), tumors/tissues at the site of transplantation were dissected and analysed for the human-origin cells using human-specific antigen CD298 expression

by flow cytometry (Figure 3D). Surprisingly, explants obtained from mice transplanted with RAC1B-null MCF7 clones still contained some $CD298^+$ cells, despite the absence of tumor growth. However, unlike parental MCF7 cells recovered from xenograft tumors, RAC1B-null MCF7 cells sorted as $CD298^+$ population from the explants formed neither mammospheres nor monolayer colonies (Figure 3E,F). These results indicate that RAC1B is indispensable for BCSC self-renewal and tumor growth *in vivo*.

Taken together, our results revealed that RAC1B is essential for BCSC plasticity and chemoresistance of MCF7 cells *in vitro*, and for BCSC maintenance and tumor-initiating ability *in vivo*.

Loss of Rac1b function does not alter mammary gland development

Rac1 is indispensable for mammary gland development and function, particularly in MaSCs in nulliparous animals, lobuloalveolar development during pregnancy and tissue remodelling during involution [18, 39-42]. Since the $Rac1^{flox/flox}$ mouse line used in these studies resulted in the loss of both Rac1 and Rac1b, we generated a $Rac1b^{-/-}$ mouse line to identify Rac1b-specific loss-of function phenotypes. In both C57BL/6 and FVB backgrounds, $Rac1b^{-/-}$ mice were born with expected Mendelian ratios and had a normal life span with no apparent health problems.

To determine whether the loss of Rac1b function hampers mammary gland development, we performed whole-mount staining on No4 inguinal mammary glands of both $Rac1b^{-/-}$ mice and their wild-type littermates at different postnatal developmental stages. During pubertal stages, there were no macroscopically obvious differences in ductal outgrowth or ductal branching in 4-, 6-, 8-, and 10-week-old $Rac1b^{-/-}$ mice (Figure 4A,B). Similarly, $Rac1b^{-/-}$ mammary glands were indistinguishable from $Rac1b^{+/+}$ glands in early and late pregnancy, lactation, and involution stages (Figure 4C,D).

Next, we evaluated whether the loss of Rac1b function affects mammary epithelial lineage diversification and/or MaSC activities. Basal ($CD49f^{high}$;$CD24^{low}$) and luminal ($CD49f^{low}$;$CD24^{high}$) epithelial cell populations showed a similar distribution within the glands of 8-week-old nulliparous $Rac1b^{-/-}$, $Rac1b^{+/-}$ and $Rac1b^{+/+}$ mice as determined by flow cytometry (Supplementary Figure 2A-C). When sorted and plated in mammosphere culture, $Rac1b^{-/-}$ luminal and basal epithelial populations were indistinguishable from their $Rac1b^{+/+}$ counterparts in terms of luminal progenitor-driven acini and MaSC-driven mammosphere formation, respectively (Supplementary Figure 2D,E). These results indicate that Rac1b function is dispensable for luminal progenitor and MaSC activities.

Together, our data demonstrate that mammary gland phenotypes of Rac1-null mice [18, 39, 40] are due to the loss-of-function of Rac1, but not Rac1b. Importantly, Rac1b deficiency does not lead to any obvious alterations in MaSCs or defects in normal mammary gland development.

Rac1b expression marks a substantial subset of BCSCs and is required for BCSC maintenance

Dual loss of Rac1 and Rac1b functions in MMTV-NIC mouse model delays tumor latency in a dose-dependent manner (Figure 1E). To determine whether loss of Rac1b is responsible for the observed tumor

latency phenotype, we analysed the impact of Rac1b deficiency on palpable tumor formation using MMTV-NIC mouse model. Our results revealed that the tumor latency in $Rac1b^{-/-}$;MMTV-NIC or $Rac1b^{+/-}$;MMTV-NIC mice is similar to $Rac1b^{+/+}$;MMTV-NIC mice (Figure 5A). This indicates that the delayed tumor latency phenotype observed in $Rac1^{flox/flox}$;MMTV-NIC and $Rac1^{flox/+}$;MMTV-NIC mice is due to the loss of Rac1, not Rac1b.

Since the loss of RAC1B in MCF7 cells results in BCSC depletion *in vivo* (Figure 3F), we examined whether Rac1b is also required for BCSCs in the MMTV-NIC mouse model. We performed mammosphere assay using $CD49f^{+}CD24^{+}$ tumor cells isolated from $Rac1b^{+/+}$;MMTV-NIC (or $Rac1b^{+/-}$;MMTV-NIC) and $Rac1b^{-/-}$;MMTV-NIC tumors (Figure 5B,C). Our results revealed a 65% decrease in overall mammosphere-forming BCSC frequency in Rac1b-null tumors compared with Rac1b-proficient tumors.

To identify whether BCSCs express Rac1b in the MMTV-NIC tumors, we aimed to generate a transgenic mouse line serving as a surrogate reporter for Rac1b splicing. To this end, we utilised CRISPR-targeting approach, coupled with homology-directed repair (HDR) template, to knock-in a T2A-mRFP cassette in-frame within the exon3b of *Rac1* gene. First, we used the murine mammary epithelial cell line, EPH4, to optimise the HDR template design for achieving a successful knock-in without disrupting proper splicing of the transgenic mRNA. Single-cell EPH4 clones, generated after HDR template-coupled CRISPR targeting using three different HDR templates, were genotyped (Supplementary Figure 3A,B) and subsequently verified by sequencing. Flow cytometry analysis of these clones revealed that the insertion of the T2A-mRFP cassette in the middle or at the 5'- end, but not at the 3'-end, of exon3b results in a population of 5–6% of cells expressing mRFP (Supplementary Figure 3C). Importantly, Rac1 expression in these clones was not altered (Supplementary Figure 3D). We then used the HDR-template option-B (knocking-in the T2A-mRFP cassette into the middle of exon3b) for HDR-coupled CRISPR targeting of fertilised mouse embryos. This provided us a new transgenic mouse line, $Rac1b^{RFP/+}$. RT-PCR analysis of RFP^{+} and RFP^{-} cells sorted from mammary glands of nulliparous $Rac1b^{RFP/+}$ mice confirmed that mRFP expression in this mouse line is a valid surrogate reporter for Rac1b splicing (Supplementary Figure 3E,F).

To determine whether Rac1b is expressed by BCSCs, we crossed $Rac1b^{RFP/+}$ and MMTV-NIC mouse lines and analysed the RFP^{+} cells from the mammary tumors of double transgenic animals by flow cytometry and mammosphere assay. The RFP^{+} (i.e. Rac1b-expressing) cells from $Rac1b^{RFP/+}$;MMTV-NIC tumors constituted a small population of lineage (CD31, CD45, TER119)-negative cells (Figure 6A), which displayed a 4-fold enriched frequency of mammosphere-forming cells compared with the $Lin^{-}RFP^{-}$ population (Figure 6B and Supplementary Figure 4A). Immunostaining of primary mammospheres formed by the $Lin^{-}RFP^{+}$ cells isolated from $Rac1b^{RFP/+}$;MMTV-NIC tumors revealed that most of these mammospheres (~90%) were composed of cells expressing CK18 luminal and/or CK14 basal epithelial lineage markers (Figure 6C). These results demonstrate that a substantial subset of BCSCs in MMTV-NIC tumors express Rac1b.

To further define the composition of RFP^+ cell populations in $Rac1b^{RFP/+}$;MMTV-NIC tumors, we immunostained the sorted Lin^-RFP^+ cells for CK18 and CK14 (Supplementary Figure 4B). Our results revealed that an average of 79.3% of Lin^-RFP^+ cells were expressing CK18, whereas 2.7% were positive for both CK14 and CK18 (Figure 6D). Furthermore, the flow cytometry analysis showed that an average of 84% of the Lin^-RFP^+ cells from $Rac1b^{RFP/+}$;MMTV-NIC tumors were also $CD24^+$ (Figure 6E). These results indicate that in MMTV-NIC tumors Rac1b is expressed in a small population of tumor epithelia that also contains a substantial subset of BCSCs.

Next, we analysed Rac1b-proficient ($Rac1b^{RFP/+}$;MMTV-NIC) and Rac1b-null ($Rac1b^{RFP/-}$;MMTV-NIC) tumors to determine whether the observed decrease in overall BCSC pool in $Rac1b^{-/-}$;MMTV-NIC tumors is due to a change in RFP^+ BCSCs. In both genotypes, Lin^-RFP^+ cells were detected with similar frequency (Figure 6F). However, there were approximately 42% fewer mammosphere-forming BCSCs in the Lin^-RFP^+ population of Rac1b-null tumors compared with the same population in Rac1b-proficient tumors (Figure 6G). In contrast, mammosphere-forming efficiency of Lin^-RFP^- cells did not show a significant difference between genotypes.

Collectively, our results demonstrate that Rac1b is expressed in a substantial subset of BCSCs, which requires Rac1b function for their maintenance *in vivo*.

Loss of Rac1b increases the chemosensitivity of primary breast tumor cells.

Rac1b function is required for the chemoresistance of MCF7 cells (Figure 3A). To investigate whether Rac1b also affects chemoresistance of Neu-driven tumors, we generated primary cell lines from $Rac1b^{+/+}$;MMTV-NIC and $Rac1b^{-/-}$;MMTV-NIC tumors and treated them with either 1 uM or 2.5 uM doxorubicin for 24 hours. At both concentrations of doxorubicin, the relative cell loss was significantly higher in Rac1b-null lines compared with Rac1b-proficient lines after 24-hour treatment (Figure 7; Day 0 samples), demonstrating an increased cytotoxic response of Rac1b-null tumor cells to doxorubicin.

The sustained cytotoxic effect of doxorubicin during the first 4 days of recovery after the removal of chemotherapeutic agent was observed in both genotypes but showed a significantly higher cell loss in Rac1b-null lines for the 1uM doxorubicin-treated groups (Figure 7; Day 4 samples). Starting from Day 8 of the recovery period, most samples showed an increase in cell growth. However, the mean values for Rac1b-null lines was consistently lower than the Rac1b-proficient lines during the whole period of recovery, despite not displaying a statistical significance between genotypes due to the heterogeneity of recovery-response by individual cell lines of same genotypes (Supplementary Figure 5). Interestingly, 3 out of 4 Rac1b-null lines treated with 2.5 uM doxorubicin did not show an increase in cell numbers between Day 8 and Day 28 of recovery, whereas only 1 out of 4 Rac1b-proficient lines showed a lack of recovery during the same period (Figure 7C). These results imply that, even at lower concentrations, doxorubicin treatment achieves a higher level of cytotoxic effect in Rac1b-null tumor cells, whereas at higher doxorubicin concentrations the recovery from the chemotherapy treatment is less likely in Rac1b-null tumor lines compared with Rac1b-proficient tumor lines.

These data demonstrate that Rac1b function is required for chemoresistance of primary breast tumor cells similar as observed in MCF7 cells. This reveals that a future strategy for treating breast cancers can involve the combined use of chemotherapeutic agents together with Rac1b-selective inhibitors.

Discussion

Developing CSC-targeting treatments to ablate tumors at their root has been a research aim for over two decades. However, this idea has proven elusive in breast cancer due to high levels of heterogeneity within the BCSC pool and the lack of appropriate molecular targets showing tumor-specific stem cell selectivity for their functional indispensability. Here, we have demonstrated that RAC1B, the alternatively spliced variant of RAC1, is required for the plasticity and self-renewal of BCSCs and for the chemosensitivity of breast tumor cells. Importantly, in the normal mammary gland, Rac1b is dispensable for MaSCs and tissue development. Since loss of Rac1b function does not lead to any apparent developmental or physiological health problems *in vivo*, selective RAC1B-targeting can be a clinically relevant option to developing novel BCSC-targeted therapies.

We have also demonstrated that inhibition of overall RAC signalling results in a dramatic loss of BCSCs *in vitro*, and the loss of Rac1 function leads to a significant delay in tumor latency *in vivo* in a dose-dependent manner. However, unlike Rac1b, Rac1 function is indispensable for normal development and physiology [17-20]. Given that heterozygous Rac1-null mice have a normal and healthy lifespan, while tumor development is significantly delayed in $Rac1^{flox/+}$;MMTV-NIC mice, partial inhibition of RAC1 activity could also be considered as a potential BCSC-targeting therapy. Indeed, xenograft studies have shown beneficial effects of EHT-1864 and EHop-016 treatments in delaying tumor growth, angiogenesis and metastatic spread of breast tumor cells [43, 44]. Importantly, these studies have reported a low serum concentration of these inhibitors being still effective, though higher doses showed toxic effects in mice. Translating those findings into clinical use would require a careful assessment of effectiveness at the maximum tolerable dose of RAC inhibitors. In contrast, one may expect that any selective RAC1B inhibitors developed in future would not be subject to these strict constraints.

Although the current experimental evidence does not allow us to unequivocally link the observed RAC1B-deficiency phenotypes in BCSC plasticity, BCSC maintenance *in vivo* and increased chemosensitivity of tumor cells, we propose a hypothetical model suggesting that in the absence of RAC1B function BCSCs are switched towards (or sustained at) a proliferative state (Figure 2E). This not only makes them vulnerable to the effects of chemotherapy (Figures 3A and 7A-D), but also results in the exhaustion of BCSCs (Figures 3C-F and 6B,G) potentially due to increased numbers of cell division. Future studies to understand the underlying molecular mechanisms of how BCSCs regulate the transition between different stem cell states to maintain their plasticity may uncover the mechanistic role of RAC1B function in these processes.

While the loss of RAC1B prevents MCF7 cells from forming tumors *in vivo*, mammary tumorigenesis is not prevented by the loss of Rac1b in the MMTV-NIC mouse model, although it leads to a reduction in

BCSCs in those tumors. This might be due to an evolutionary adaptation of the Rac1b$^{-/-}$;MMTV-NIC tumors to the lack of Rac1b, whereupon tumor clones that are less dependent on Rac1b function for their growth gain a selective advantage during the initial stages of tumorigenesis. Future studies could use Rac1b-selective inhibitors or temporally-controlled genetic deletion approaches (i.e CreERT-mediated deletion of floxed-Rac1b alleles) to assess whether therapeutic intervention to inhibit Rac1b activity in Rac1b-expressing breast tumors could provide an additional clinical benefit further than increasing the chemosensitivity of breast tumors.

Materials And Methods

Mouse experiments:

All mouse experiments were conducted under license in accordance with the UK Home Office Animals (Scientific Procedures) Act (1986) regulations with the approval of study protocols by the Animal Welfare and Ethical Review Body (AWERB) of the University of Manchester. Mice were maintained in a pathogen-free facility at the University of Manchester and kept in 12h light-dark cycles in temperature- and humidity-controlled environment and were provided with food and water ad libitum.

The mouse lines Rac1^{flox} and MMTV-NIC were previously described [32, 33]. Rac1b$^{-/-}$ mouse line was generated by crossing the Rac1b$^{flox/flox}$ mice [16] with a universal CRE-deleter mouse line[45] and subsequently breeding out the CRE-transgene and backcrossing into C57BL6/J and FVB/J backgrounds for at least 7 generations. Rac1b$^{RFP/+}$ mouse line in pure FVB/J background has been generated in this study using HDR-coupled CRISPR-targeting as described below. Xenograft transplantations of MCF7 cells in immunodeficient nude mice were performed as previously described [46].

Mice at defined pregnancy stages were obtained by timed mating with the morning of vaginal plug observation being considered as 0.5 days-post-coitum (d.p.c). Whole-mount staining of No4 mammary glands were performed as described elsewhere [47].

Generation of Rac1bRFP mouse line by CRISPR-Cas9:

CRISPR sgRNA sequences targeted proximally to the insert site (TGTCTCCAACCTAGTAATGC and GGTAAAGATAGACCCTCCAG) were purchased as crRNA oligos and annealed with tracrRNA (both oligos supplied by Integrated DNA Technologies) in sterile, RNase free injection buffer (TrisHCl 1mM, pH 7.5, EDTA 0.1mM) by combining 2.5 ug crRNA with 5 ug tracrRNA and heating to 95^{o}C, which was allowed to slowly cool to room temperature. For our donor repair template, we used the EASI-CRISPR long-ssDNA strategy [48], and generated a homology flanked lssDNA donor using protocols described in [49].

For embryo microinjection the annealed sgRNA was complexed with Cas9 protein (New England Biolabs) at room temperature for 10 minutes, before addition of long ssDNA donor (final concentrations; sgRNA 20 ng/ul, Cas9 protein 20 ng/ul, lssDNA 10 ng/ul). CRISPR reagents were directly microinjected into FVB

(Envigo) zygote pronuclei using standard protocols. Zygotes were cultured overnight and single-cell embryos surgically implanted into the oviduct of day 0.5 post-coitum pseudopregnant mice.

Potential founder mice were screened by PCR, first using primers that flank the sgRNA sites (Frw: tccagctgcatggagtaatg, Rev: gcagcctctcctgagtgagt), which both identifies editing activity in the form of InDels from NHEJ repair in almost every pup and can also detect larger products implying HDR. Secondary PCRs used the same primers in combination with mRFP1 primers (mRFP1_R: cgccctcgatctcgaact, mRFP1_F: ccgaggtcaagaccacctac). A founder giving positive products in all three PCR reactions was further characterised by Sanger sequencing of the PCR amplicons of the initial PCR.

Mammosphere-formation assay:

Single cells were plated in 96 well ultra-low attachment plates in sphere-forming medium as described in [50]. For cell lines, cells were plated at a concentration of 1 000 cells/ml and 10 000 cells/ml. For cells sorted from mammary glands, they were plated at a concentration of 10 000 cells/ml and 100 000 cells/ml. Primary tumor cells were plated at a concentration of 50 000 cells/ml and 100 000 cell/ml. Mammosphere numbers were quantified at Day 5 or Day 7 of mammosphere culture of cell lines or primary cells, respectively. Solid structures with a minimum diameter of 50 um on two perpendicular axes are considered as mammospheres.

Statistical analysis:

Statistical tests used in this study were selected based on population distribution, data type and sample centrality/variability to meet assumptions of tests using GraphPad Prism and Microsoft Excel software. P values <0.05 were considered statistically significant. Data are expressed as mean ± standard deviation (SD) or mean ± standard error of the mean (SEM).

All other methods used in this study are described in the Supplementary methods.

Declarations

ACKNOWLEDGEMENTS

This work was supported by scientific fellowship grant (#2016MaySF722) to A.U and project grant (#2013MayPR029) to C.S from Breast Cancer Now. We thank Marzieh Kamjoo, Miaomiao He and Rognvald Blance for technical support; Peter March (Bioimaging) and Mike Jackson (Flow Cytometry) for core research facility support; staff at the University of Manchester Biological Safety Unit for looking after the mice; Olga Ucar for proofreading and Karen Blyth for academic mentorship to A.U.

AUTHOR CONTIBUTIONS

F.C., C.S, and A.U developed the concept of this study, analysed the data and wrote the manuscript. R.C, K.B, and C.T contributed to the study design and data interpretation. D.N contributed to the cell line work; D.A performed the xenograft transplantations, K.P, J.Z, and S.E contributed to the method optimisations and data acquisition; N.H and A.A contributed to the generation of knock-in mouse line; A.C generated the Rac1b knockout mouse line; F.C and A.U performed all other experiments in this study.

CONFLICT OF iNTEREST

The authors declare no competing interests.

References

1. Sung, H., et al., *Global Cancer Statistics 2020: GLOBOCAN Estimates of Incidence and Mortality Worldwide for 36 Cancers in 185 Countries.* CA Cancer J Clin, 2021. **71**(3): p. 209-249.
2. McDermott, S.P. and M.S. Wicha, *Targeting breast cancer stem cells.* Mol Oncol, 2010. **4**(5): p. 404-19.
3. Fritz, G., et al., *Rho GTPases in human breast tumours: expression and mutation analyses and correlation with clinical parameters.* Br J Cancer, 2002. **87**(6): p. 635-44.
4. Kamai, T., et al., *Overexpression of RhoA, Rac1, and Cdc42 GTPases is associated with progression in testicular cancer.* Clin Cancer Res, 2004. **10**(14): p. 4799-805.
5. Engers, R., et al., *Prognostic relevance of increased Rac GTPase expression in prostate carcinomas.* Endocr Relat Cancer, 2007. **14**(2): p. 245-56.
6. Pan, Y., et al., *Expression of seven main Rho family members in gastric carcinoma.* Biochem Biophys Res Commun, 2004. **315**(3): p. 686-91.
7. Porter, A.P., A. Papaioannou, and A. Malliri, *Deregulation of Rho GTPases in cancer.* Small GTPases, 2016. **7**(3): p. 123-38.
8. De, P., J.C. Aske, and N. Dey, *RAC1 Takes the Lead in Solid Tumors.* Cells, 2019. **8**(5).
9. Cardama, G.A., et al., *Relevance of small GTPase Rac1 pathway in drug and radio-resistance mechanisms: Opportunities in cancer therapeutics.* Crit Rev Oncol Hematol, 2018. **124**: p. 29-36.
10. Hofbauer, S.W., et al., *Tiam1/Rac1 signals contribute to the proliferation and chemoresistance, but not motility, of chronic lymphocytic leukemia cells.* Blood, 2014. **123**(14): p. 2181-8.
11. Hein, A.L., et al., *RAC1 GTPase promotes the survival of breast cancer cells in response to hyper-fractionated radiation treatment.* Oncogene, 2016. **35**(49): p. 6319-6329.
12. Dokmanovic, M., et al., *Rac1 contributes to trastuzumab resistance of breast cancer cells: Rac1 as a potential therapeutic target for the treatment of trastuzumab-resistant breast cancer.* Mol Cancer Ther, 2009. **8**(6): p. 1557-69.
13. Zhao, Y., et al., *Inactivation of Rac1 reduces Trastuzumab resistance in PTEN deficient and insulin-like growth factor I receptor overexpressing human breast cancer SKBR3 cells.* Cancer Lett, 2011. **313**(1): p. 54-63.

14. Sun, J., et al., *RAC1 plays an essential role in estrogen receptor alpha function in breast cancer cells.* Oncogene, 2021. **40**(40): p. 5950-5962.
15. Rosenblatt, A.E., et al., *Inhibition of the Rho GTPase, Rac1, decreases estrogen receptor levels and is a novel therapeutic strategy in breast cancer.* Endocr Relat Cancer, 2011. **18**(2): p. 207-19.
16. Gudino, V., et al., *RAC1B modulates intestinal tumorigenesis via modulation of WNT and EGFR signalling pathways.* Nat Commun, 2021. **12**(1): p. 2335.
17. Desai, L.P., et al., *RhoA and Rac1 are both required for efficient wound closure of airway epithelial cells.* Am J Physiol Lung Cell Mol Physiol, 2004. **287**(6): p. L1134-44.
18. Olabi, S., et al., *Integrin-Rac signalling for mammary epithelial stem cell self-renewal.* Breast Cancer Res, 2018. **20**(1): p. 128.
19. Wells, C.M., et al., *Rac1-deficient macrophages exhibit defects in cell spreading and membrane ruffling but not migration.* J Cell Sci, 2004. **117**(Pt 7): p. 1259-68.
20. Satoh, M., et al., *Requirement of Rac1 in the development of cardiac hypertrophy.* Proc Natl Acad Sci U S A, 2006. **103**(19): p. 7432-7.
21. Marei, H. and A. Malliri, *Rac1 in human diseases: The therapeutic potential of targeting Rac1 signaling regulatory mechanisms.* Small GTPases, 2017. **8**(3): p. 139-163.
22. Wertheimer, E., et al., *Rac signaling in breast cancer: a tale of GEFs and GAPs.* Cell Signal, 2012. **24**(2): p. 353-362.
23. Haga, R.B. and A.J. Ridley, *Rho GTPases: Regulation and roles in cancer cell biology.* Small GTPases, 2016. **7**(4): p. 207-221.
24. Jordan, P., et al., *Cloning of a novel human Rac1b splice variant with increased expression in colorectal tumors.* Oncogene, 1999. **18**(48): p. 6835-9.
25. Schnelzer, A., et al., *Rac1 in human breast cancer: overexpression, mutation analysis, and characterization of a new isoform, Rac1b.* Oncogene, 2000. **19**(26): p. 3013-20.
26. Zhou, C., et al., *The Rac1 splice form Rac1b promotes K-ras-induced lung tumorigenesis.* Oncogene, 2013. **32**(7): p. 903-9.
27. Fiegen, D., et al., *Alternative splicing of Rac1 generates Rac1b, a self-activating GTPase.* J Biol Chem, 2004. **279**(6): p. 4743-9.
28. Manuel Iglesias, J., et al., *Mammosphere formation in breast carcinoma cell lines depends upon expression of E-cadherin.* PLoS One, 2013. **8**(10): p. e77281.
29. Onesto, C., et al., *Characterization of EHT 1864, a novel small molecule inhibitor of Rac family small GTPases.* Methods Enzymol, 2008. **439**: p. 111-29.
30. Montalvo-Ortiz, B.L., et al., *Characterization of EHop-016, novel small molecule inhibitor of Rac GTPase.* J Biol Chem, 2012. **287**(16): p. 13228-38.
31. Pece, S., et al., *Biological and molecular heterogeneity of breast cancers correlates with their cancer stem cell content.* Cell, 2010. **140**(1): p. 62-73.

32. Walmsley, M.J., et al., *Critical roles for Rac1 and Rac2 GTPases in B cell development and signaling.* Science, 2003. **302**(5644): p. 459-62.
33. Ursini-Siegel, J., et al., *ShcA signalling is essential for tumor progression in mouse models of human breast cancer.* EMBO J, 2008. **27**(6): p. 910-20.
34. Sugihara, K., et al., *Rac1 is required for the formation of three germ layers during gastrulation.* Oncogene, 1998. **17**(26): p. 3427-33.
35. Shutes, A., et al., *Specificity and mechanism of action of EHT 1864, a novel small molecule inhibitor of Rac family small GTPases.* J Biol Chem, 2007. **282**(49): p. 35666-78.
36. Dharmawardhane, S., E. Hernandez, and C. Vlaar, *Development of EHop-016: a small molecule inhibitor of Rac.* Enzymes, 2013. **33 Pt A**: p. 117-46.
37. Liu, S., et al., *Breast cancer stem cells transition between epithelial and mesenchymal states reflective of their normal counterparts.* Stem Cell Reports, 2014. **2**(1): p. 78-91.
38. Nie, S., et al., *A quantitative proteomics analysis of MCF7 breast cancer stem and progenitor cell populations.* Proteomics, 2015. **15**(22): p. 3772-83.
39. Bagci, H., et al., *Impaired cell death and mammary gland involution in the absence of Dock1 and Rac1 signaling.* Cell Death Dis, 2014. **5**: p. e1375.
40. Akhtar, N., et al., *Rac1 Controls Both the Secretory Function of the Mammary Gland and Its Remodeling for Successive Gestations.* Dev Cell, 2016. **38**(5): p. 522-35.
41. Akhtar, N. and C.H. Streuli, *Rac1 links integrin-mediated adhesion to the control of lactational differentiation in mammary epithelia.* J Cell Biol, 2006. **173**(5): p. 781-93.
42. Moreno-Layseca, P., et al., *The requirement of integrins for breast epithelial proliferation.* Eur J Cell Biol, 2017. **96**(3): p. 227-239.
43. Castillo-Pichardo, L., et al., *The Rac Inhibitor EHop-016 Inhibits Mammary Tumor Growth and Metastasis in a Nude Mouse Model.* Transl Oncol, 2014. **7**(5): p. 546-55.
44. Hampsch, R.A., et al., *Therapeutic sensitivity to Rac GTPase inhibition requires consequential suppression of mTORC1, AKT, and MEK signaling in breast cancer.* Oncotarget, 2017. **8**(13): p. 21806-21817.
45. Schwenk, F., U. Baron, and K. Rajewsky, *A cre-transgenic mouse strain for the ubiquitous deletion of loxP-flanked gene segments including deletion in germ cells.* Nucleic Acids Res, 1995. **23**(24): p. 5080-1.
46. Simoes, B.M., et al., *Anti-estrogen Resistance in Human Breast Tumors Is Driven by JAG1-NOTCH4-Dependent Cancer Stem Cell Activity.* Cell Rep, 2015. **12**(12): p. 1968-77.
47. Ucar, A., et al., *miR-212 and miR-132 are required for epithelial stromal interactions necessary for mouse mammary gland development.* Nat Genet, 2010. **42**(12): p. 1101-8.
48. Quadros, R.M., et al., *Easi-CRISPR: a robust method for one-step generation of mice carrying conditional and insertion alleles using long ssDNA donors and CRISPR ribonucleoproteins.* Genome Biol, 2017. **18**(1): p. 92.

49. Bennett, H., E. Aguilar-Martinez, and A.D. Adamson, *CRISPR-mediated knock-in in the mouse embryo using long single stranded DNA donors synthesised by biotinylated PCR.* Methods, 2021. **191**: p. 3-14.
50. Ucar, A., et al., *Adult thymus contains FoxN1(-) epithelial stem cells that are bipotent for medullary and cortical thymic epithelial lineages.* Immunity, 2014. **41**(2): p. 257-69.

Figures

FIGURE 1

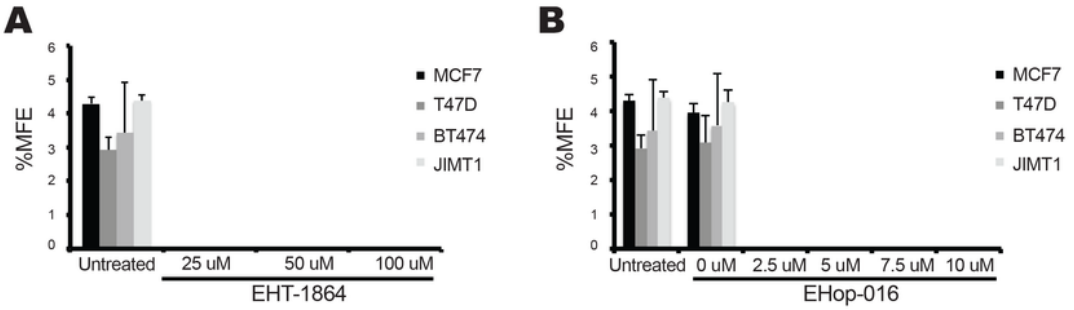

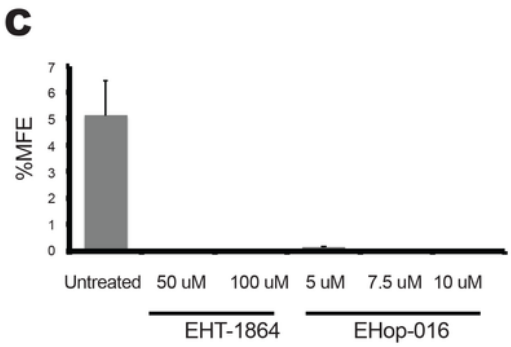

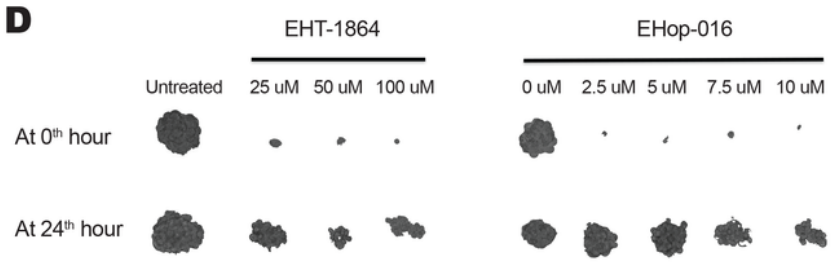

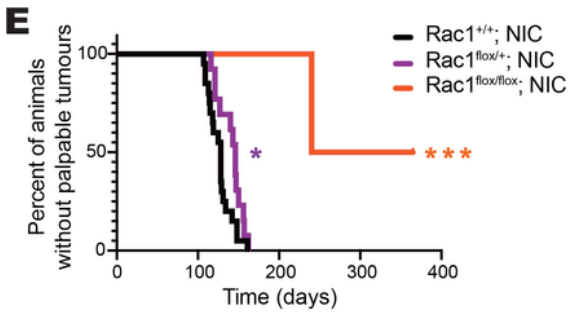

	Rac1$^{+/+}$;NIC/+	Rac1$^{flox/+}$;NIC/+	Rac1$^{flox/flox}$;NIC/+
Median	128	146	302.5

Figure 1

RAC activity is required for BCSCs *in vitro* and breast tumorigenesis *in vivo*.

A,B) The effect of RAC-specific inhibitors EHT-1864 **(A)** and EHop-016 **(B)** on the mammosphere-forming efficiency (%MFE) of human breast cancer cell lines (MCF7, T47D, BT474, and JIMT1) for the indicated

concentrations of inhibitors were quantified. Values represent the mean ± SD of 3 independent experiments.

C) Mammosphere-forming efficiency (%MFE) for the secondary mammosphere culture of MCF7 cells, which were treated with the indicated concentrations of EHT-1864 or EHOP-016 during their primary mammosphere cultures, were quantified in the absence of corresponding inhibitors in culture. Values represent the mean ± SD of 3 independent experiments.

D) Representative images of structures formed by MCF7 cells that are treated with the indicated concentrations of EHT-1864 or EHop-016 in the mammosphere culture either starting from the time of plating (0 hour) or added at the 24^{th} hour of culture. In **(A)**, **(B)**, and **(D)**, the EHop-016 treatment group of '0 uM' corresponds to vehicle-only group, which is the same DMSO concentration as in '10 uM' treatment group.

E) Tumor latency analysis for $Rac1^{+/+}$;MMTV-NIC (n=20), $Rac1^{flox/+}$;MMTV-NIC (n=13), $Rac1^{flox/flox}$;MMTV-NIC (n=2) mice. Time represents postnatal age in days. Median age of palpable tumor formation for each genotype is shown below the graph. P values (*: $p<0.05$; ***: $p<0.01$) were calculated using Lox-rank Mantel Cox test.

FIGURE 2

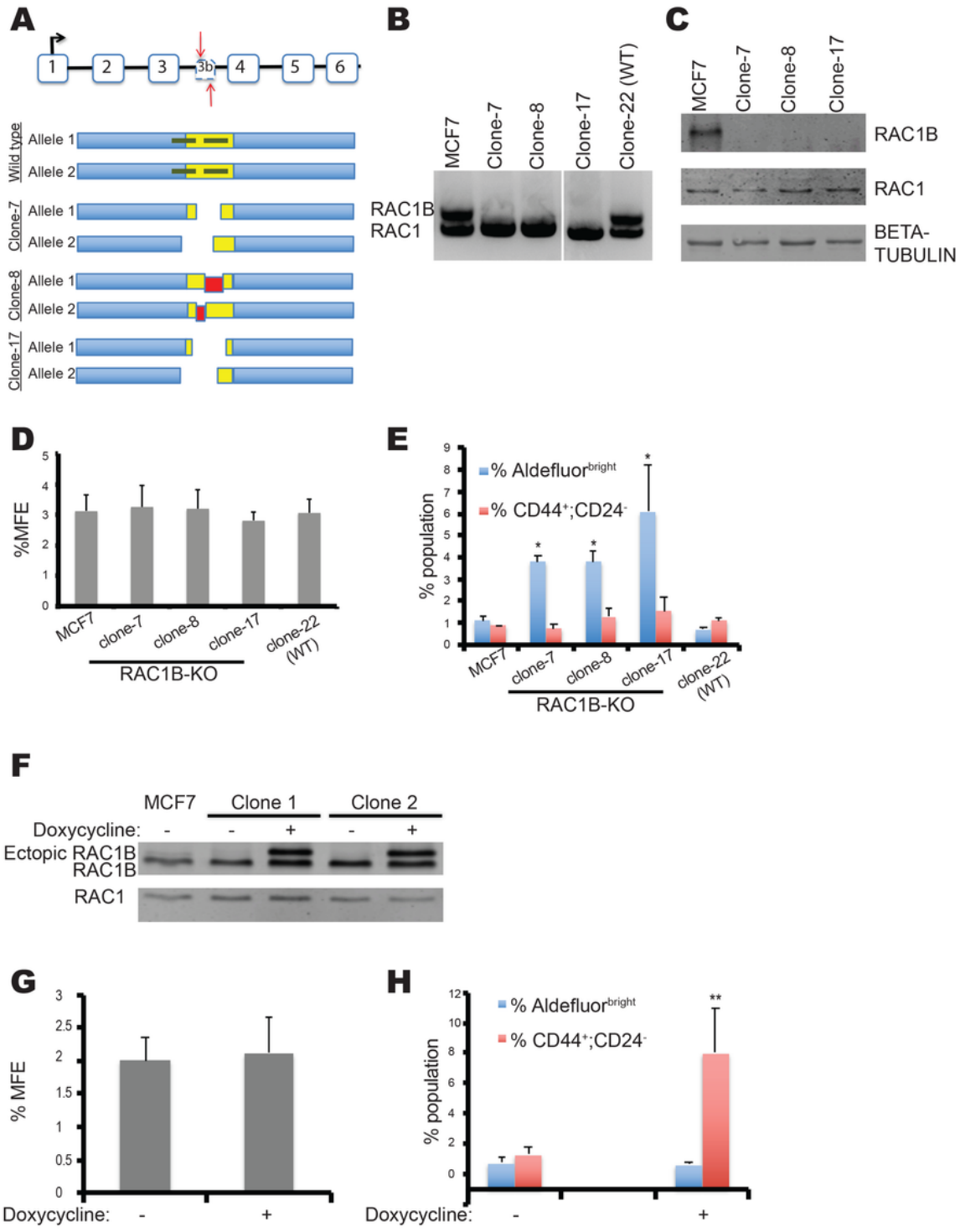

Figure 2

RAC1B regulates BCSC plasticity without altering the size of BCSC pool in MCF7 cells.

A) Schematic representation of CRISPR/Double nickase targeting strategy and allelic maps showing indel mutations generated in each independent single-cell MCF7 clone. Vertical red arrows on the upper image of exon map of *RAC1* gene and the green horizontal lines in the allele map of wildtype clone marks the

targeted genomic sites by sgRNA sequences used. In allele maps, the exon3b sequence is depicted in yellow and the flanking intronic sequences in blue; gaps correspond to deletions, whereas the regions shown in red corresponds to insertions.

B,C) RT-PCR **(B)** and immunoblot analysis **(C)** of single-cell clones. Beta-tubulin was used as a loading control in immunoblot experiments.

D) Mammosphere-forming efficiency (%MFE) of parental MCF7 and single-cell clones. Values represent the mean ± SD of 3 independent experiments. There was no significant difference between any clones (two-tailed paired t-test).

E) Percentage of cells that form Aldefluor^{bright} or CD44^{+};CD24^{-} populations in parental MCF7 and single-cell clones as determined by flow cytometry analyses. Values represent the mean ± SD of 3 biological replicates. *: p<0.05, one-tailed paired t-test for comparison of each clone to parental MCF7 sample.

F) Immunoblot analysis of stable-transgenic MCF7 clones with doxycycline-inducible RAC1B overexpression that are treated with or without 2 ug/ml doxycycline.

G) Mammosphere-forming efficiency (%MFE) of stable-transgenic MCF7 clones with doxycycline-inducible RAC1B overexpression that are treated with or without 2 ug/ml doxycycline. Values represent the mean ± SD of 3 independent experiments.

H) Percentage of cells that form the Aldefluor^{bright} and CD44^{+};CD24^{-} populations in the stable-transgenic MCF7 clones with doxycycline-inducible RAC1B overexpression that are treated with or without 2 ug/ml doxycycline.**: p<0.01, one-tailed paired t-test

FIGURE 3

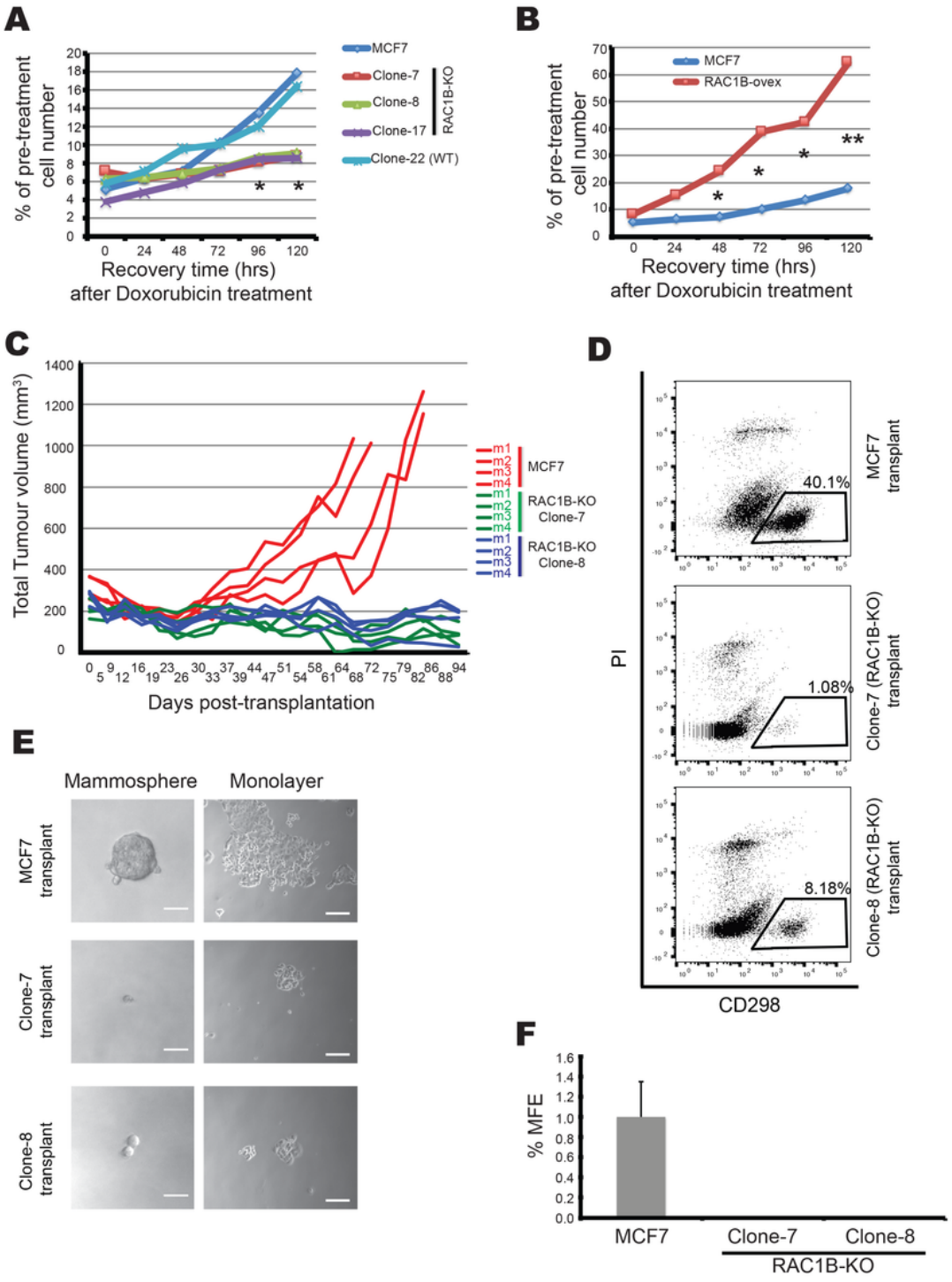

Figure 3

RAC1B function is essential for chemo-resistance *in vitro* and tumor formation *in vivo*.

A) Cell growth curve of parental MCF7, RAC1B-proficient Clone 22 and three RAC1B-null single-cell clones in post-treatment recovery period after 2.5 uM doxorubicin treatment for 24 hours. Cell numbers are presented as percentage of the pre-treatment cell number in each sample. Each data point represents the

mean of three independent experiments. Significant difference was observed for each RAC1b-null clone compared with both parental MCF7 and RAC1B-proficient clone only at 96- and 120-hours post-treatment recovery time (*: $p<0.05$, two-tailed unpaired t-test).

B) Cell growth curve of stable-transgenic MCF7 clones with doxycycline-inducible RAC1B overexpression treated with (RAC1B-ovex) or without (MCF7) 2.5 uM Doxycycline in post-recovery period after 2.5 uM Doxorubicin treatment for 24 hours. Percentage cell number calculations are as described in (**A**). Each data point represents the mean of three independent experiments. Significant differences (*: $p<0.05$; **:$p<0.01$, two-tailed unpaired t-test) were observed at 48-, 72-, 96- and 120-hours post-treatment recovery time (*: $p<0.05$; **:$p<0.01$, two-tailed unpaired t-test).

C) Tumor growth *in vivo* for the xenograft transplantation assay. Hundred thousand cells of parental MCF7 or two different RAC1B-null MCF7 clones were transplanted into both right and left dorsal sides of 4 immunodeficient nude mice per group, and tumor volumes were measured twice weekly with callipers. The data represent the total tumor volume for each individual mouse.

D) Flow cytometry analysis of the transplants described in (**C**). Representative dot plots show single cells stained with propidium iodide (PI) as dead cell marker and CD298 as a human specific antigen used for distinguishing the cells of human origin.

E) Representative images of mammosphere and monolayer cultures of $CD298^+$ cells sorted from transplants as shown in (**D**). Scale bars represent 50 um and 100 um for mammosphere and monolayer cultures, respectively.

F) Mammosphere-forming efficiency (%MFE) of $CD298^+$ cells sorted from transplants as shown in (**D**). Of note, the data for MCF7 is the mean ± SD for three animals, whereas for Rac1B-null clones the data represents %MFE of pooled cell samples from 3 explants of the same single-cell clone.

FIGURE 4

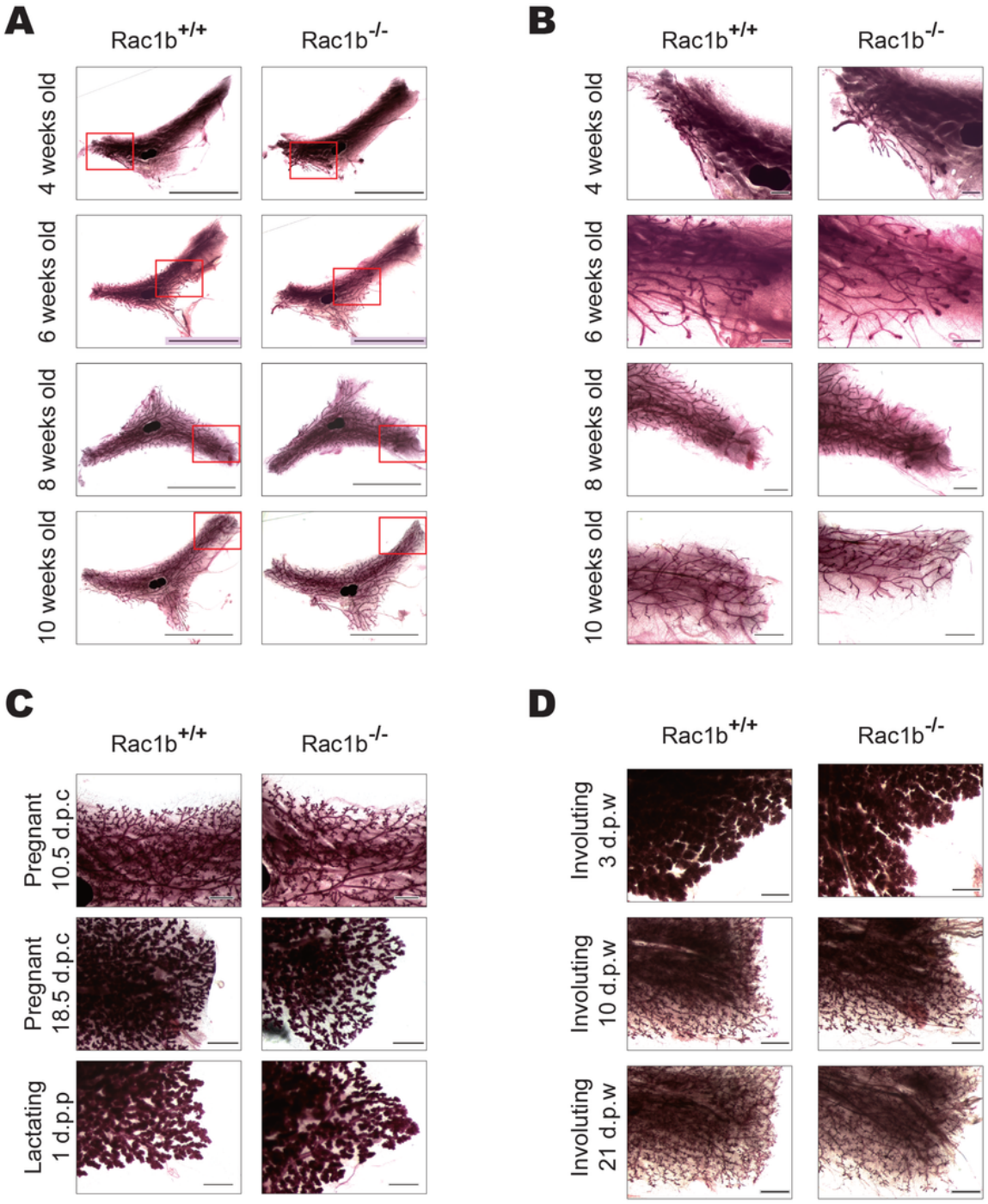

Figure 4

Rac1b is dispensable during mammary gland development

A) Representative images of whole-mount stained mammary glands of 4-, 6-, 8-, and 10-week-old nulliparous Rac1b$^{+/+}$ and Rac1b$^{-/-}$ mice.

B) Higher magnification images of distal parts of the ductal tree at locations depicted with a rectangle in (**A**).

C) Representative images of whole-mount stained mammary glands of Rac1b$^{+/+}$ and Rac1b$^{-/-}$ mice at developmental stages of early pregnancy (10.5 d.p.c [days post-coitum]), late pregnancy (18 d.p.c.), and lactation (Day 1 d.p.p [days post-partum]).

D) Representative images of whole-mount stained mammary glands of Rac1b$^{+/+}$ and Rac1b$^{-/-}$ mice at involution stages of 3, 10 and 21 days post-weaning (d.p.w).

Scale bars represent 1 cm in (**A, C, D**) and 1 mm in (**B**). Images shown are representative of n³3 mice.

FIGURE 5

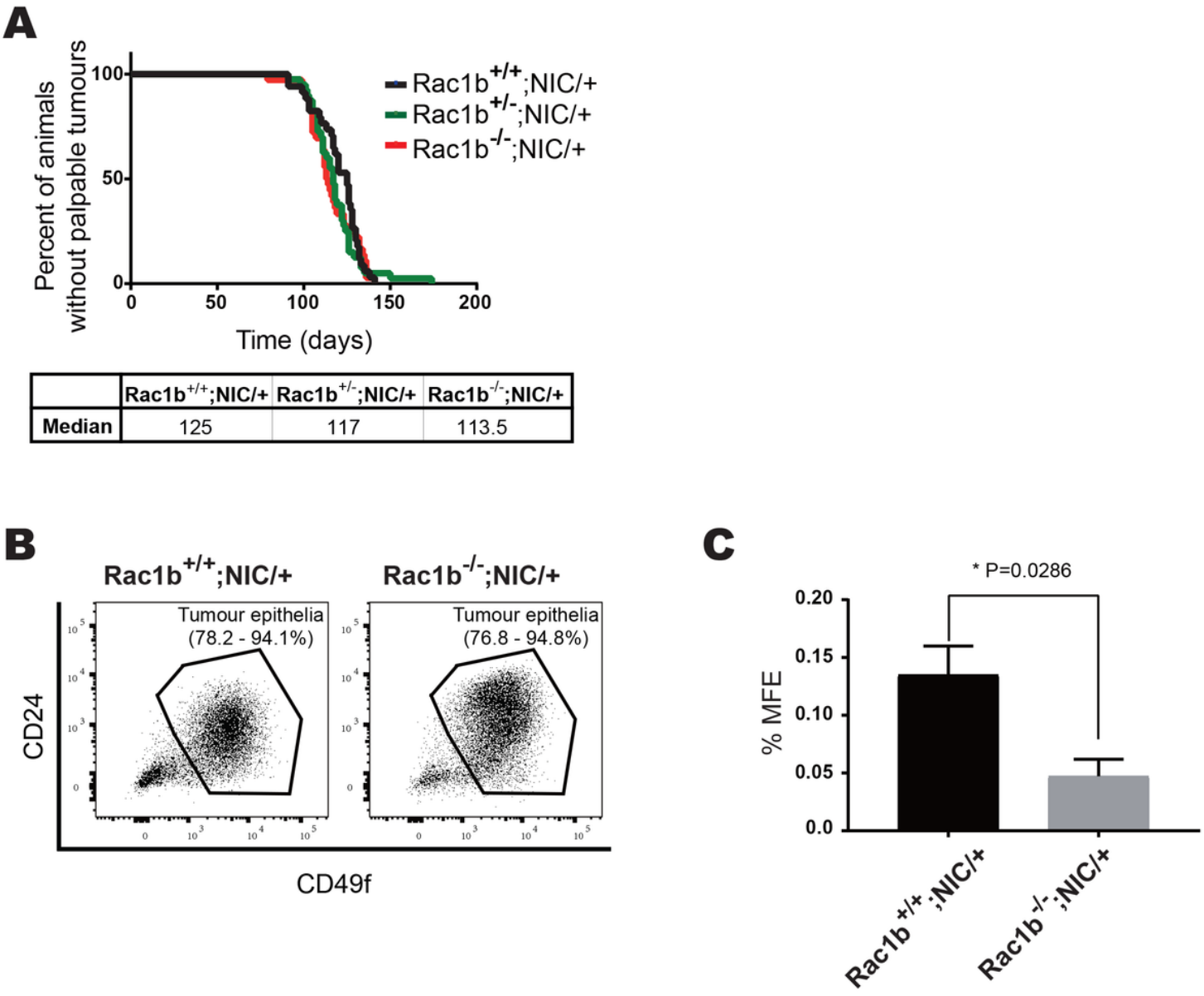

	Rac1b$^{+/+}$;NIC/+	Rac1b$^{+/-}$;NIC/+	Rac1b$^{-/-}$;NIC/+
Median	125	117	113.5

Figure 5

Loss of Rac1b function results in decreased BCSC frequency without altering tumor latency.

A) Tumor latency analysis for Rac1b$^{+/+}$;MMTV-NIC (n=34), Rac1b$^{+/-}$;MMTV-NIC (n=40), Rac1b$^{-/-}$;MMTV-NIC (n=36) mice. Time represents postnatal age in days. Median age of palpable tumor formation for each genotype is shown below the graph. There were no statistically significant differences between genotypes according to the Lox-rank Mantel Cox test.

B) Representative dot plots of CD49f versus CD24 expression for flow cytometry analysis of primary mammary cells of Rac1b$^{+/+}$;MMTV-NIC and Rac1b$^{-/-}$;MMTV-NIC mice are shown for the single, alive, lineage-negative cell population. The observed range for tumor epithelial cell frequency of different animals of same genotype is shown above the CD49f^{+};CD24^{+} gate (n=9).

C) Mammosphere forming efficiency (%MFE) of tumor epithelial cell populations sorted from Rac1b$^{+/+}$;MMTV-NIC and Rac1b$^{-/-}$;MMTV-NIC tumors as shown in (**B**). Values represent the mean ± SEM of 5 animals. P value obtained by the paired t-test is shown on the graph.

FIGURE 6

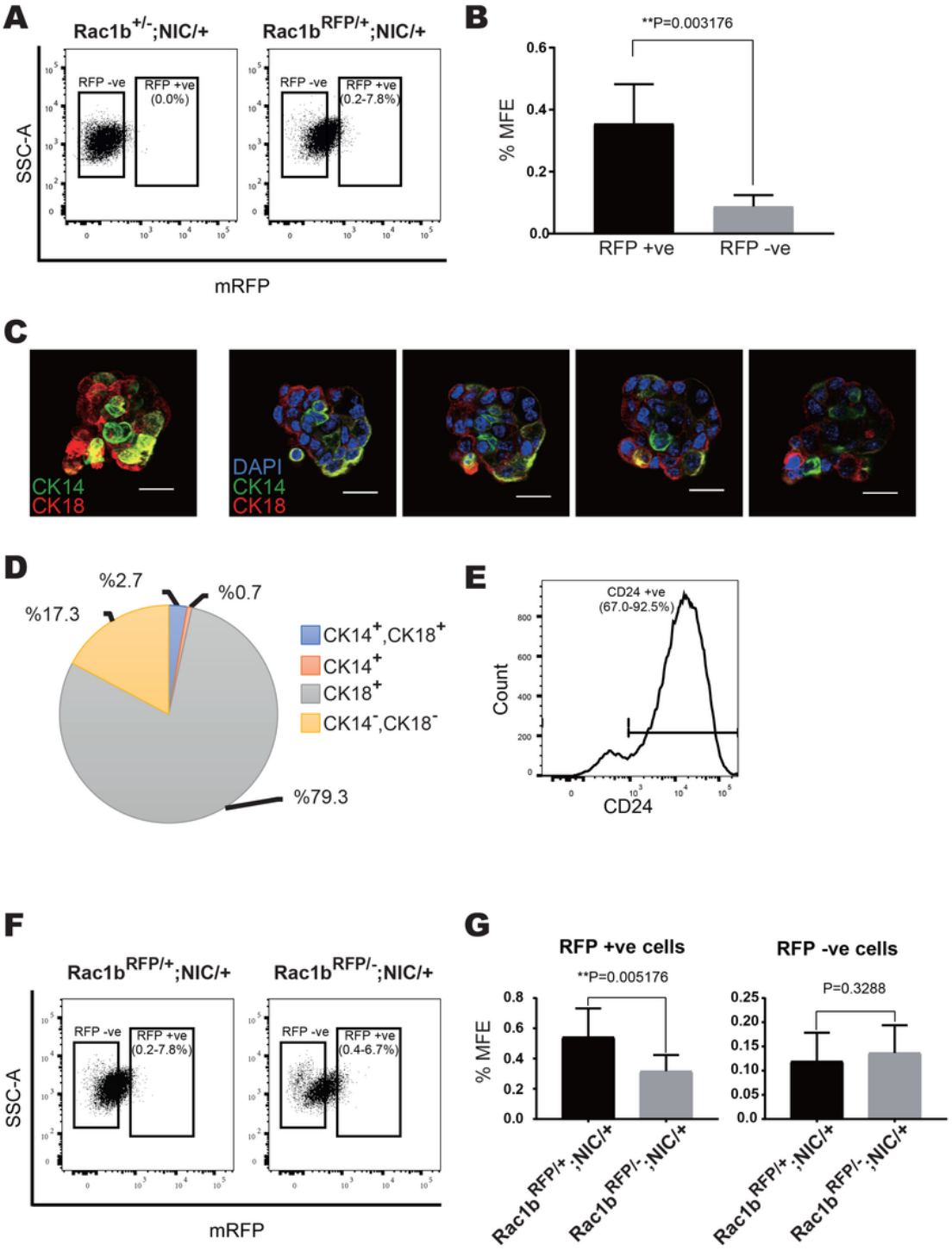

Figure 6

Rac1b function is required for the maintenance of a large subset of BCSCs expressing Rac1b.

A) Representative dot plots for flow cytometry analysis of primary tumor cells from Rac1b$^{+/-}$;MMTV-NIC and Rac1b$^{RFP/+}$;MMTV-NIC mice are shown for the single, alive, lineage-negative cell population. The observed range for RFP^{+} cell frequency between different animals is shown within the RFP^{+} gate (n=6).

B) Mammosphere forming efficiency (%MFE) of RFP^+ versus RFP^- cells sorted from $Rac1b^{RFP/+}$;MMTV-NIC tumors as shown in (**A**). Values represent the mean ± SEM of 6 animals. P value obtained by the paired t-test is shown on the graph.

C) Representative confocal microscopy images of a primary mammosphere formed by Lin^-RFP^+ tumor cells sorted from $Rac1b^{RFP/+}$;MMTV-NIC breast tumors (n=3 mice) and coimmunostained for CK18 and CK14 expression. The leftmost image shows the deconvoluted image for CK14 (green) and CK18(red). Individual images of confocal planes selected to represent different Z-stack positions are shown together with DAPI-staining (shown in blue) serving as a nuclear stain. Scale bars represent 20 um.

D) Pie chart representation for the distribution of CK-18 and/or CK-14 expressing Lin^-RFP^+ tumor cells sorted from $Rac1b^{RFP/+}$;MMTV-NIC breast tumors. Values represent the mean of 3 animals.

E) Representative histogram of flow cytometric analysis of CD24 expression by the Lin^-RFP^+ cells sorted from $Rac1b^{RFP/+}$;MMTV-NIC tumors (n=3). The observed range for the $CD24^+$ cell frequency is shown on the graphs.

F) Representative dot plots for flow cytometry analysis of primary tumor cells of $Rac1b^{RFP/+}$;MMTV-NIC and $Rac1b^{RFP/-}$;MMTV-NIC mice are shown for the single, alive, lineage-negative cell population. The observed range of RFP^+ cell frequency of different animals of same genotype is shown within the RFP^+ gate (n=9).

G) Mammosphere forming efficiency (%MFE) of RFP^+ versus RFP^- cells sorted from $Rac1b^{RFP/+}$;MMTV-NIC and $Rac1b^{RFP/-}$;MMTV-NIC tumors as shown in (**F**). Values represent the mean ± SEM of 3 animals. P values obtained by the paired t-test are shown on the graphs.

FIGURE 7

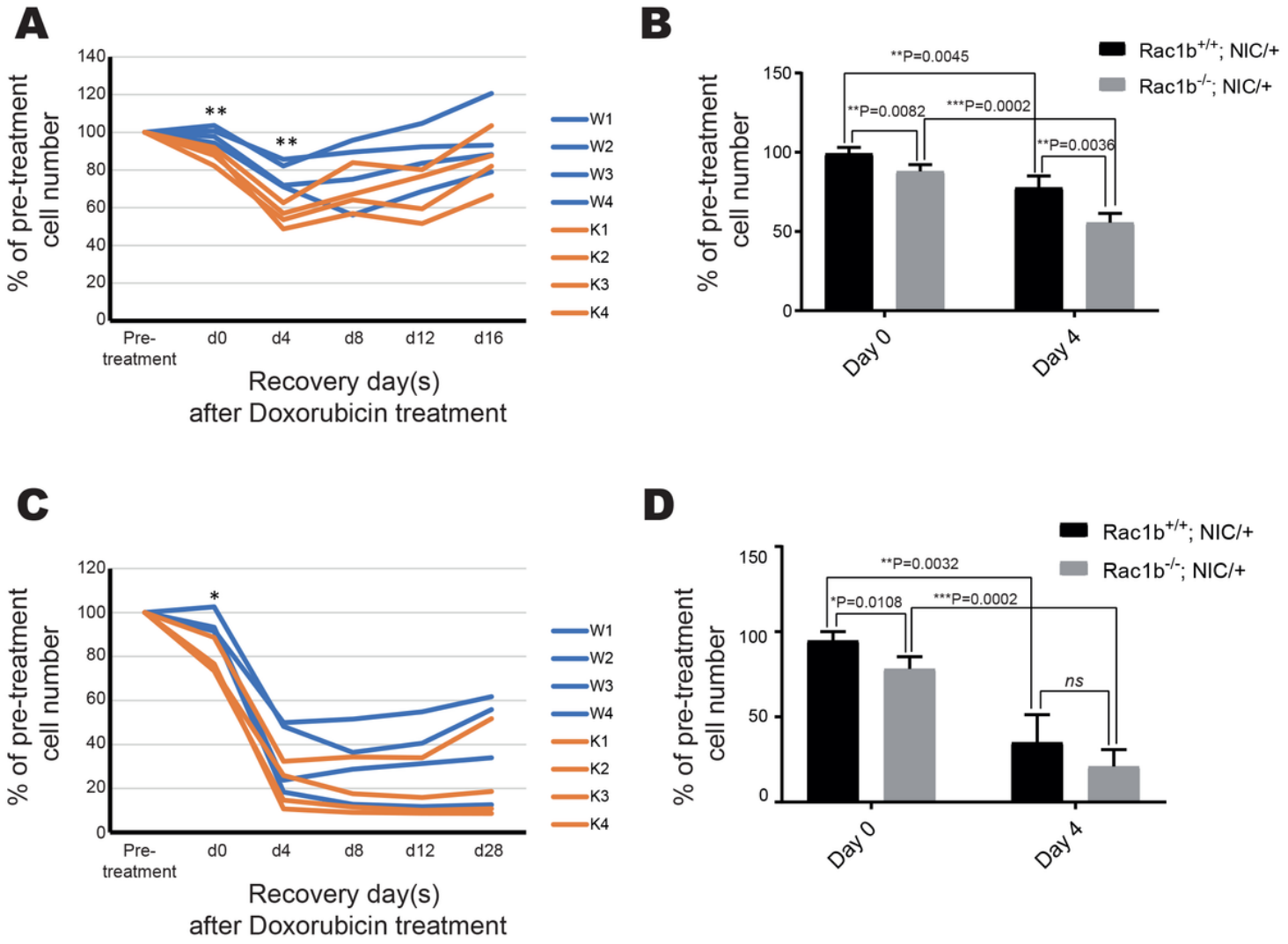

Figure 7

Loss of Rac1b function increases the chemosensitivity of primary breast tumor cells

A,B) Cell growth curve of primary tumor cell lines obtained from Rac1b$^{+/+}$;MMTV-NIC (n=4) and Rac1b$^{-/-}$;MMTV-NIC (n=4) breast tumors in post-treatment recovery period after 1 uM (**A**) or 2.5uM (**B**) Doxorubicin treatment for 24 hours. Cell numbers are normalised to the pre-treatment cell number in each sample and represented as percentage. Each data point represents the mean of three independent experiments. Statistical significance was calculated using two-tailed unpaired t-test. (*: $p<0.05$ and **: $p<0.01$)

C,D) Bar graph representation of the cell growth data shown in (**A**) and (**B**) to provide a statistical comparison of data at Day 0 and Day 4 of post-treatment recovery period. P values obtained by two-

tailed unpaired t-test for comparisons between genotypes or recovery time points are depicted on the graph. Values represent the mean ± SD of 4 independent primary cell lines, ns: not significant

Supplementary Files

This is a list of supplementary files associated with this preprint. Click to download.

- FCSupplementaryInformation.pdf